물리탐사
Vol. 6, No. 4, 2003, p. 199~206

Characteristics of Static Shift in 3-D MT Inversion

Tae Jong Lee[1], Toshihiro Uchida[2], Yutaka Sasaki[3] and Yoonho Song[1]

3차원 MT 역산에서 정적효과의 특성 고찰

이태종[1] · 内田 利弘[2] · 佐久木 裕[3] · 송윤호[1]

Abstract : Characteristics of the static shift are discussed by comparing the three-dimensional MT inversion with/without static shift parameterization. The galvanic distortion by small-scale shallow feature often leads severe distortion in inverted resistivity structures. The new inversion algorithm is applied to four numerical data sets contaminated by different amount of static shift. In real field data interpretations, we generally do not have any a-priori information about how much the data contains the static shift. In this study, we developed an algorithm for finding both Lagrangian multiplier for smoothness and the trade-off parameter for static shift, simultaneously in 3-D MT inversion. Applications of this inversion routine for the numerical data sets showed quite reasonable estimation of static shift parameters without any a-priori information. The inversion scheme is successfully applied to all the four data sets, even when the static shift does not obey the Gaussian distribution. Allowing the static shift parameters have non-zero degree of freedom to the inversion, we could get more accurate block resistivities as well as static shifts in the data. When inversion does not consider the static shift as inversion parameters (conventional MT inversion), the block resistivities on the surface are modified considerably to match possible static shift. The inhomogeneous blocks on the surface can generate the static shift at low frequencies. By those mechanisms, the conventional 3-D MT inversion can reconstruct the resistivity structures to some extent in the deeper parts even when moderate static shifts are in the data. As frequency increased, however, the galvanic distortion is not frequency independent any more, and thus the conventional inversion failed to fit the apparent resistivity and phase, especially when strong static shift is added. Even in such case, however, reasonable estimation of block resistivity as well as static shift parameters were obtained by 3-D MT inversion with static shift parameterization.

Keywords : 3-D MT inversion, static shift, static shift parameterization

요 약 : MT 탐사자료의 역산에 있어서 지하의 전기비저항과 함께 정적효과를 파라미터로 설정하여 동시 역산을 수행하는 알고리듬을 하나의 지하구조 모델에 각기 다른 양의 정적효과를 포함시킨 4개의 자료에 대하여 적용시키고 이를 정적효과가 전혀 고려되지 않은 경우와 비교하여, 3차원 역산에서 정적효과가 미치는 영향 및 그 특성에 대하여 분석하였다. 일반적으로 현장자료에 정적효과가 어느 정도 포함되어 있는지에 대한 사전 정보가 전혀 없으므로 역산과정에서 이를 조절하는 trade-off 파라미터의 적절한 선택이 매우 중요하며, 본 연구에서는 모델의 smoothness와 static shift 의 양을 조절하는 각각의 파라미터의 크기를 매 반복마다 구하는 알고리듬을 동시역산에 적용하였으며 4개의 이론자료에 적용한 결과 만족할 만한 결과를 얻었다. 정적효과가 포함된 자료에 대하여 정적효과를 고려하지 않은 역산(기존의 MT 역산)에서는 지표 block의 전기비저항을 바꿔 역산 스스로가 정적효과를 유발하려는 경향을 보였으며 이의 결과로 저주파수에서는 상당한 정적효과를 발생시켜 정적효과가 그리 크지 않은 경우 심부구조를 어느 정도 규명해 내는 것으로 나타났다. 그러나 고주파수에서는 이들 지표 block의 영향이 주파수에 무관하지 않게 되어 정적효과를 포함하는 자료의 겉보기 전기비저항과 위상을 동시에 만족시키지 못하게 된다. 그러나 정적효과를 파라미터로 하는 동시역산의 경우, 매우 심한 정적효과를 포함하는 자료에 대해서도 지하구조를 매우 정확히 영상화 하는 것이 가능하였다.

주요어 : 3차원 MT 역산, 정적효과, 정적효과 파라미터

*2003년 11월 3일 접수
1) 한국지질자원연구원(Korea Institute of Geoscience and Mineral Resources, Daejeon 305-350, Korea)
2) 일본 산업기술총합연구소(Institute of Geo-Resources and Environment, AIST, Tsukuba 305-8567, Japan)
3) 일본 큐슈대학(Kyushu Univ.)

Introduction

Magnetotelluric (MT) have found frequent applications in geological studies of the upper and lower crust, and in mineral, hydrocarbon, and geothermal resources explorations (Kurtz *et al.*, 1993; Romo *et al.*, 1997; Uchida *et al.*, 2000, 2001), due to its good depth penetration. Galvanic distortion (Groom and Bailey, 1989), however, prevents more wide spread acceptance and application of the method. It is usually caused by the presence of charges on local, small scale, shallow, lateral inhomogenities. The charge built up at the interfaces of small scale near-surface inhomogenities compared to the penetration depth of the EM field produces *frequency-independent* distortion of electric fields (see, for example, deGroot-Hedlin, 1991). The distortion affects on the electric field only, so that it appears as parallel shifts in MT sounding curves when plotted in log (apparent resistivity) vs. log (period) scale. The phenomenon is called "static shift" and often ranges over three orders of magnitude, which is frequently observed in resistive crystalline terrains (Kurtz *et al.*, 1993). Because the entire data is affected by small-scale shallow feature, the static shift will lead severe distortion in inverted resistivity structures. Removing static shift is a critical problem and will vastly improve interpretation of MT data.

Various methods for static shift removal have been developed as is summarized in Sternberg *et al.* (1988). They can be loosely divided into three categories: 1) spatial filtering by closely spaced MT sites, i.e., Electro-Magnetic Array Profiling (EMAP: Torres-Verdin, 1991, Bostick, 1986), 2) theoretical calculations of the static shift from buried near-surface inhomogeneities or surface topographic effects (Wannamaker *et al.*, 1984; Jones, 1988), 3) use of auxiliary data from known geology or independent measurement such as TEM coincident sounding (Sternberg *et al.*, 1988). All of these techniques have successively applied to static shift compensation. They, however, may be prohibitively costly to acquire the extra-data at the necessary number of sites, particularly in large regional surveys.

Alternative method, which does not require additional information, was suggested by DeGroot-Hedlin (1991). It solves simultaneously for static shift parameters as well as block resistivities as inversion parameters. This method assumes that total sum of static shift parameters, for all sites and modes, is close to zero. Ogawa and Uchida (1996) improved it to take into account two types of constraint on the nature of static shift. A regularized inversion is performed to solve simultaneously for the block resistivities and static shifts at each receiving points, which produces the smoothest model. By allowing static shifts to be free parameters, smooth inversion ensures that structures appearing in the models are not simply due to the incorrect removal of static shift. Sasaki (2001) applied the static shift parameterization to 3-D MT inversion using finite difference forward calculation (Sasaki, 1999).

Based on Sasaki's code, in this paper, some modifications are made to the code and characteristics of static shift are considered using a numerical model with varying static shift contents in the data. The modifications are mainly in two categories; one is to add weighting based on the errors in the data, and the other is to add a routine for searching best trade-off parameter for static shift. At first in this paper, we will discuss about a little detail about static shifts, and the theory of smooth inversion scheme will be followed. And then numerical examples will be demonstrated.

Static shift

Figure 1 shows a typical apparent resistivity curves for 21 sites of MT data collected for crustal sounding over a crystalline basement (Kurtz et al., 1993). Three orders of magnitude of static shift is manifest in that all the profiles are

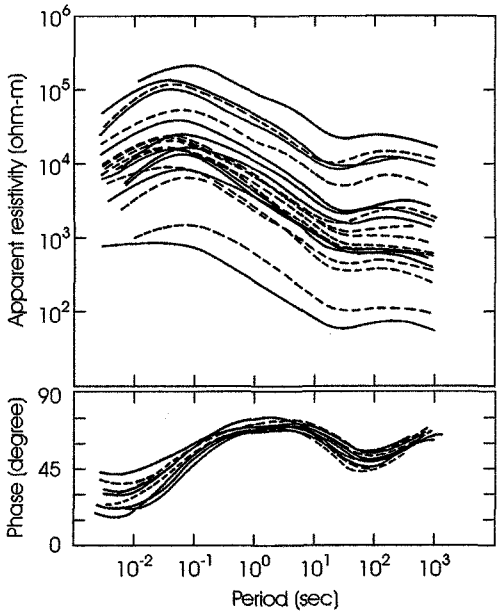

Fig. 1. Typical apparent resistivity curves for 21 sites of MT data collected for crustal sounding over a crystalline basement (from Kurtz *et al.*, 1993). All the resistivity curves are roughly parallel but show vertical displacement from each other.

roughly parallel, but show vertical displacement from each other.

The secondary electric field set up by the boundary charges (LeMouel and Menvielle, 1982)

$$\mathbf{E}_s=-\frac{\partial \mathbf{A}_s}{\partial t}-\nabla\phi \tag{1}$$

where $\mathbf{A}_s$ is the secondary magnetic vector potential resulting from the boundary charges and ϕ is the electrostatic potential. If the inhomogeneity is small compared to the penetration depth of the EM field, the first term in equation (1) is negligible so that by Coulomb's law (deGroot-Hedlin, 1991)

$$\mathbf{E}_s=-\nabla\phi=\frac{-1}{4\pi}\int_V \frac{\mathbf{E}_p\cdot\nabla\sigma}{\sigma|\mathbf{r}|^2}\mathbf{r}_0 dv \tag{2}$$

From equation (2) it can be seen that the secondary electric field is proportional to the primary field, and that the two are in phase. Note that the secondary electric field is independent of frequency. The effect of near surface inhomogeneities is thus to scale the electric field by a multiplicative factor. For frequencies that are sufficiently low, the size of the inhomogeneity is small with respect to the wavelength within the inhomogeneity, it can be shown that the magnetic field is unaffected by the buildup of boundary charges (Wannamaker *et al.*, 1984). Thus,

$$\rho_a^{obs}=k\left|\frac{E^{obs}}{H}\right|=k\left|\frac{\alpha E'}{H}\right|=\alpha\left[k\left|\frac{E'}{H}\right|\right]=\alpha\rho_a' \tag{3}$$

where ρ_a' is undistorted apparent resistivity, which represents the real structure. The boundary charges accumulation depends not only on the conductivity of the anomaly but also the direction of electric field (TE or TM mode). The static shift is thus a function of site location and its mode. But at high frequencies, when the skin depth is less than the scale size of the inhomogeneity, the first term in equation (1) is not negligible and the effect is no longer frequency independent.

Finally, taking logarithm in both side of equation (3),

$$\log\rho_a^{obs}=\log\rho_a'+g \tag{4}$$

This means that the static shift appears as up/down shift of MT sounding curves in log-log plot.

Parameterization of static shift

By the analogy of equation (4), the MT data in the presence of static shift **s** can be described as

$$\mathbf{d}=\mathbf{F}(\mathbf{m})+\mathbf{G}\mathbf{s}, \tag{5}$$

where **d** is the calculated data, **F** is a non-linear function describing forward MT problem for a given model **m**, and **G** is a matrix relating the static shift values to the data. The rows of **G** corresponding to phase or tipper data, which will not be affected by static shift, are identically zero: and the rows corresponding to the apparent resistivities have unity at the appropriate locations. The MT problem is non-linear in that we need to solve it iteratively as follows,

$$\Delta\mathbf{d}=\mathbf{d}^{obs}-\mathbf{F}(\mathbf{m}^{(k)})=\mathbf{A}\Delta\mathbf{m}^{(k)}+\mathbf{G}\mathbf{s} \tag{6}$$

$$\mathbf{m}^{(k+1)}=\mathbf{m}^{(k)}+\Delta\mathbf{m}^{(k)} \tag{7}$$

where **A** is the Jacobian matrix. On Occam's inversion scheme, the objective function to be minimized is defined as

$$U=\left\|\mathbf{W}[\Delta\mathbf{d}\cdot\mathbf{A}\Delta\mathbf{m}^{(k)}\cdot\mathbf{G}\mathbf{s}]\right\|^2+\lambda^2\left(\left\|\mathbf{C}\mathbf{m}^{(k+1)}\right\|+\alpha^2\|\Delta\mathbf{m}\|+\beta^2\|\mathbf{s}\|^2\right) \tag{8}$$

where the first term represents data misfit, the second represents the constraints to control the smoothness of the solution, the term with α represents the Marquadt constraint, and the last constraints on the static shift. The minimization of the objective function is equivalent to solve the following matrix equations,

$$\begin{bmatrix}\mathbf{WA} & \mathbf{WG}\\ \lambda\mathbf{C} & \mathbf{0}\\ \lambda\alpha\mathbf{I} & \mathbf{0}\\ \mathbf{0} & \lambda\beta\mathbf{I}\end{bmatrix}\begin{bmatrix}\Delta\mathbf{m}\\ \mathbf{s}\end{bmatrix}=\begin{bmatrix}\mathbf{W}\Delta\mathbf{d}\\ -\lambda\mathbf{C}\mathbf{m}^{(k)}\\ \mathbf{0}\\ \mathbf{0}\end{bmatrix} \tag{9}$$

where **W** is weights related to the observation errors, **d** is observed apparent resistivity and phase, **m** is desired 3-D resistivity model, **F** is a non-linear function for forward MT problem, **C** is a roughening matrix, **s** is a vector representing the static shift at each site (TE and TM), and λ and β are tradeoff parameters for roughness and static shift, respectively. Here, it is applied a constraint that the static shift **s** statistically has a Gaussian distribution (Ogawa and Uchida, 1996). The modified Gram-Schmidt method is used to solve equation (9). Starting from the starting model $\mathbf{m}_0$, iteration is continued until desired level of misfit is achieved. The rms misfit is given by

$$rms=\sqrt{\Delta\mathbf{d}^T\mathbf{W}^T\mathbf{W}\Delta\mathbf{d}/N} \tag{10}$$

Simultaneous searching for the best tradeoff parameter λ

and β, in this study, is done to find the best model and static shift parameters based on the rms misfit at each iteration. The two parameters are closely related to each other as in equation (8). The parameter λ controls the smoothness of the inverted model as well as the amount of static shift in the form of $\lambda \times \beta$.

The forward computation **F(m)** for a given model **m** is done by staggered grid finite difference method (FDM) (Sasaki, 1999). And the Jacobian calculated from analytic solutions for a homogeneous half-space (initial model) is used to reduce the computational burden.

Finally, the block resistivity for inversion is taken logarithm. Thus the sensitivities should be modified as bellows

$$\frac{\partial f}{\partial \ln \rho_m} = -\sigma_m \frac{\partial f}{\partial \sigma_m} \tag{11}$$

where ρ_m and σ_m is the resistivity and the conductivity of the model block, respectively.

Numerical data

Figure 2 shows a model configuration for the test model, which has a conductor of 10 ohm-m and a resistor of 1000 ohm-m in a homogeneous background of 100 ohm-m. The two bodies have the same size of 1.0×1.5×1.0 km. Sixty three measurement points with 500 m spacing in x and y directions are located on the surface. Six frequencies from 0.3 Hz to 100 Hz are used. At each measuring point, apparent resistivity and phase for TE (x-y) and TM (y-x) mode are gathered, which makes 1512 known data. 3% of random noise is added to both the log-resistivity and phase in radian.

Four data sets are prepared depending on the amount of static shift contamination; 1) without static shift (Dataset0), 2) random Gaussian static shift of zero mean, standard deviation of 0.3 (Dataset1), and 0.9 (Dataset2), 3) non-Gaussian static shift (Dataset3), respectively. In Dataset 1, static shift ranges from -0.75 to 0.64, which correspond to 0.47 and 1.90 times, respectively in apparent resistivity. And in Dataset 2, from -2.25 to 1.92, which correspond to 0.1 and 6.8 times in apparent resistivity, respectively. For the inversion, the earth is discretized into 891 (11×9×9) blocks as shown with bold lines in Figure 2. The starting model for the inversion is 100 ohm-m half-space for all the Datasets.

In general cases, we do not have any a-priori information about how much the data contain the static shift and it is

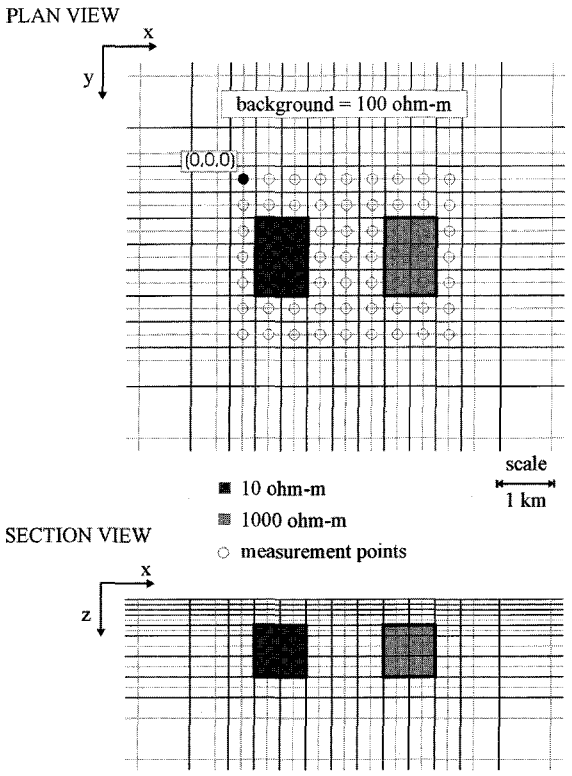

Fig. 2. A plan view and section view for the test model in this study. Two anomalous bodies with the same size of 1 km * 1.5 km * 1 km are located in the same depth of 1 km in homogeneous bedrock of its resistivity 100 ohm-m. The resistivity of a conductor is 10 ohm-m and the other body have 1000 ohm-m, respectively. Three percent of random Gaussian noise is added to the forward data.

controlled by the trade-off parameter for static shift β in the inversion. Appropriate value for β is, thus, needed for the 3-D inversion with static shift parameterization. In this study, we first compare the errors in static shift parameters with two different method of searching the trade-off parameters λ and β: 1) searching only for λ with fixing β fixed to a constant values and 2) simultaneous searching for λ and β in each iteration. The results are summarized in Table 1. The errors in estimation of static shift parameters are calculated by

$$\sum_{i=1}^{Nsite} \sum_{j=1}^{2} (s_{ij}^{E} - s_{ij}^{S})^2 / \sum_{i=1}^{Nsite} \sum_{j=1}^{2} (s_{ij}^{G})^2 \times 100(\%) \tag{12}$$

where s denotes the static shift in logarithm, the superscript E and G represents "estimated" and "given", respectively.

In Dataset1, the best estimation for the static shift in fixed β mode is made at β=2. It shows bigger errors in both β=1 and β=4. From the result we can estimate the best choice of β will be around 2 and the 2-D search resulted in β=1.82

Table 1. Comparison of rms errors in estimation of static shift parameters with fixed static shift parameter β and the simultaneous searching for λ and β at the final iteration

	Fixed β, searching for λ only				2-D search for λ and β	
β	1	2	4	8	rms	β
Dataset1	2.27%	**1.71%**	2.41%	3.08%	**1.79%**	1.82
Dataset2	**2.09%**	3.85%	7.96%	12.0%	**1.92%**	0.94

at the final iteration. Dataset2 contains bigger amount of static shift than Dataset1 and shows best estimate of static shift when β=1 in fixed β mode. Overall trend of the estimation error shows that the best choice of β will be less than 1 in this case and the 2-D search showed 0.94 at the final iteration. In general, the greater the data carry the static shift components the smaller β is needed to estimate the static shift parameter properly. And the simultaneous search for the λ and β at each iteration can help us to figure out the amount of static shift contamination in the data.

Dataset0

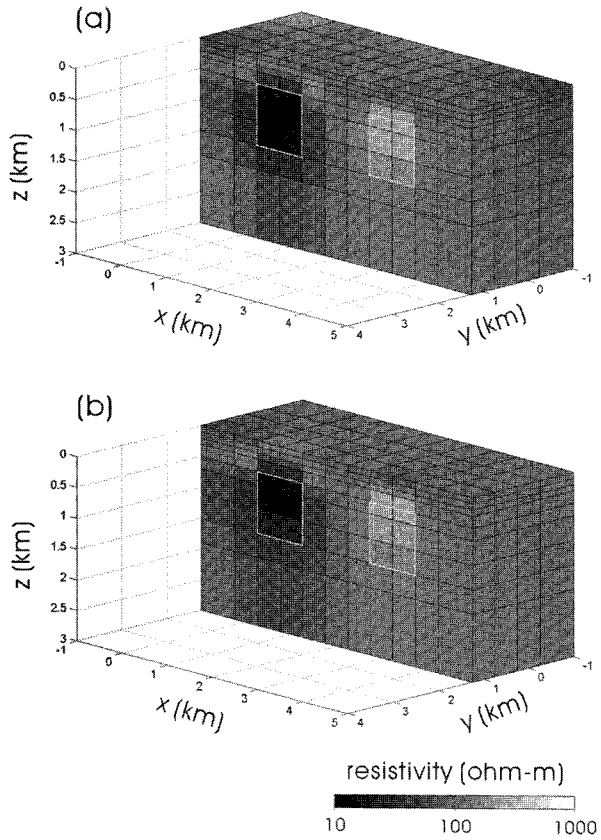

Fig. 3. Reconstructed images for the dataset0, no static shift is added. The inversion with (a) and without (b) static shift parameters shows reasonable estimation of block resistivities.

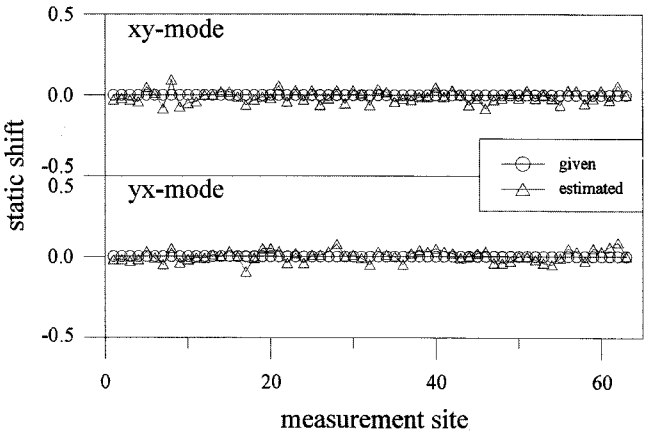

Fig. 4. Estimated static shift parameters for the dataset0, no static shift is added. The estimated values of static shift in each site show close to the given value of zero.

Dataset1 contains only 3% random noise and is not contaminated by static shift. However for the sake of checking the robustness of the algorithm, inversions including/excluding the static shift parameter are performed. Figure 3 shows the results that solve for both block resistivity with static shift parameters (a) and for the block resistivity only (b). The true models are superimposed by white squares on the figure. The initial λ and β is given by 5.0 and 4.0, and the final was 2.96 and 3.4, respectively after 6 iterations. The rms misfit reduces from 5.22 to 0.887. Because no static shift is added to the data, the block resistivities are well defined in both of the image. Figure 4 shows estimated static shift for xy and yx modes at each 63 site. Estimated static shift is essentially zero for all the sites and note that the estimated static shift parameters approach closely to zero.

Dataset1

The same experiment is performed for Dataset1. Figure 5 shows the block resistivities from the two inversion schemes, and Figure 6 shows estimated static shift parameters for the two modes at each site. As can be seen in Figure 6, the inversion estimates static shift parameters quite well and the block resistivity from the scheme separates the deep seated conductor and the resistor quite well. Note that all the surface blocks show almost homogeneous of 100 ohm-m. Physically static shift mainly occurs by the inhomogeneities on the surface. In that case the phase also should be changed as frequency getting high. At high frequencies, when the skin depth is less than the scale size of the inhomogeneity, the static effect is no longer frequency indepen-

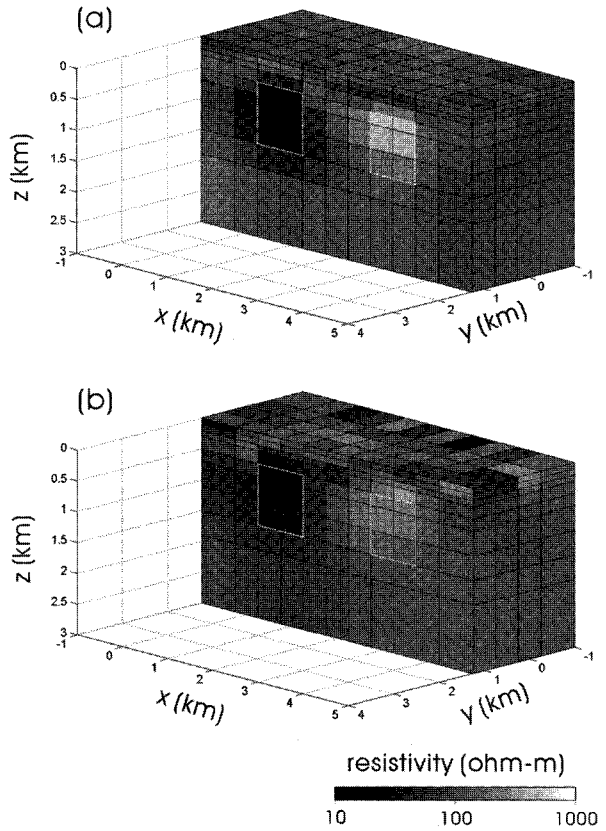

Fig. 5. Reconstructed images for the dataset1, 3% of Gaussian static shifts are added. The inversion with static shift parameters (a) shows reasonable estimation of block resistivities. But when the static shift parameters are not allowed (b), the inversion tries to generates static shift by modifying the resistivity of surface blocks.

dent. In this study, however, the static shift are given to the apparent resistivity only, which can be occurred when there exists surface inhomogeneities with very small size, the dimension is smaller than the skin depth at highest frequency measured.

Conventional inversion result in Figure 5(b) shows very complex surface inhomogeneities. It seems that the inversion tried to generate static shifts by modifying the resistivity of surface blocks. And by this, the inversion reconstructed the deeper structures conductor and the resistor to some extent.

Figure 7 compares the simulated apparent resistivity and phase data with the observed ones for the result shown in Figure 5(b). One can find typical static shift effect at low frequencies from both of the figure. The calculated and observed apparent resistivity shows parallel up/down movement independent of the frequency, while the phase shows very good match. Though the inversion tried to remove the static shift by changing the resistivity of the surface block, the static shift still remains. Note that the inversion fails to

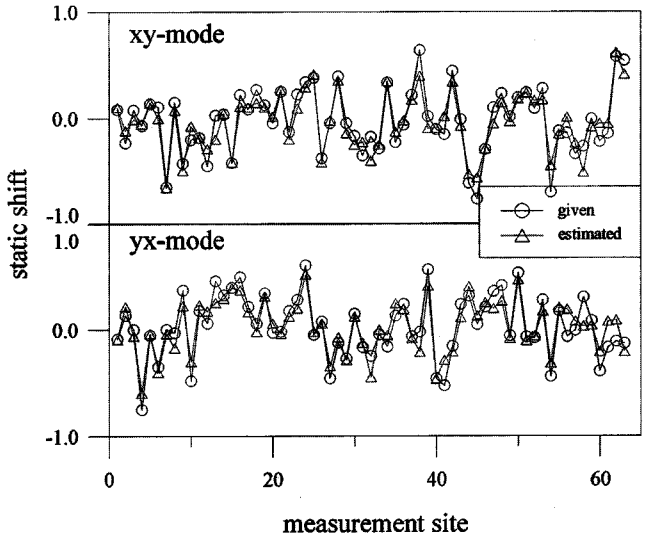

Fig. 6. Estimated static shift parameters for the dataset1, 3% random Gaussian static shifts are added. Note that the estimated static shift closely approaches to the given values.

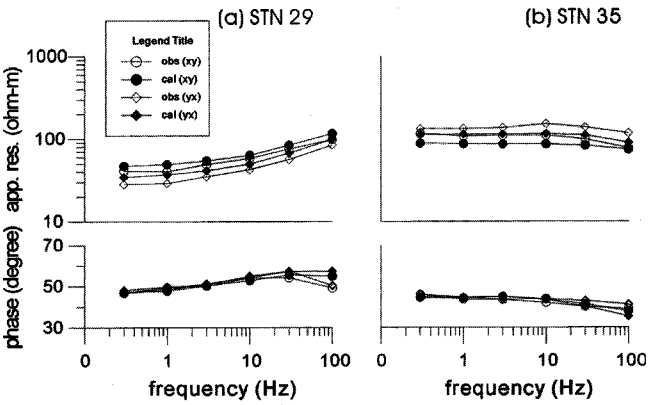

Fig. 7. Comparison between observed and calculated responses at stations 29 and 35 for the inversion driven the result in Figure 5(b). The conventional inversion tried to generate the static shift by changing the resistivity of the surface blocks. It however fails to fit the phase data at high frequencies above 30 Hz in both stations.

fit the phase data at high frequencies above 30 Hz. Changing the block resistivity on the surface causes the distortion of phase at high frequency.

Dataset2

Figure 8 and Figure 9 shows the block resistivity and estimated static shift, respectively. Even when the data is contaminated by severe the static shift, the simultaneous inversion scheme removes the static shift effect very well as shown in Figure 9, and separates the conductor and resistor quite reasonably (Figure 8a). Note that the surface blocks forms no more a homogeneous layer. Though the inversion

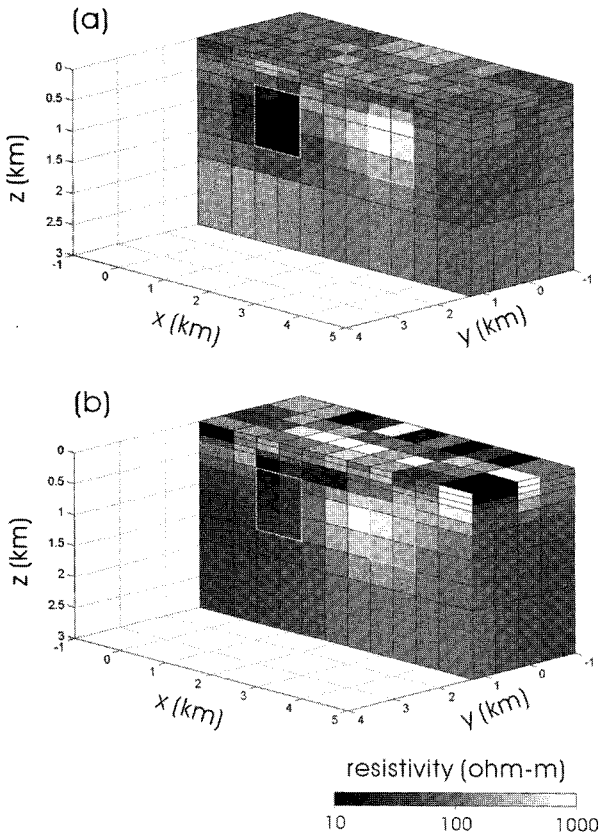

Fig. 8. Reconstructed images for the dataset2, 9% of Gaussian static shifts are added. The inversion with static shift parameters (a) shows reasonable estimation of block resistivities, while conventional inversion (b) shows complex surface structures and smeared image for the deep structures.

scheme estimated the static shift quite well, the residual in static shift is still remain. The inversion tried to fit the residual by modifying the resistivity of surface blocks as the case in Dataset1.

In this case, conventional inversion dealing with only the block resistivity fails as shown in Figure 8(b). It does not separate the two anomalous bodies. In this model, static shift from 0.1 to 6.8 times in apparent resistivity is added. Considering fact that it often ranges over three orders of magnitude (Kurtz et al., 1993), static shift should be taken into account to prevent misinterpretation of the deep structures.

Static shift with non-Gaussian distribution (Dataset3)

The inversion scheme is applied a constraint that the static shift **s** statistically has a Gaussian distribution. Finally let us see what happens when the static shift do not obey a Gaussian distribution. Figure 10 shows the given and estimated static shift when the static shift occurs only in yx-mode of

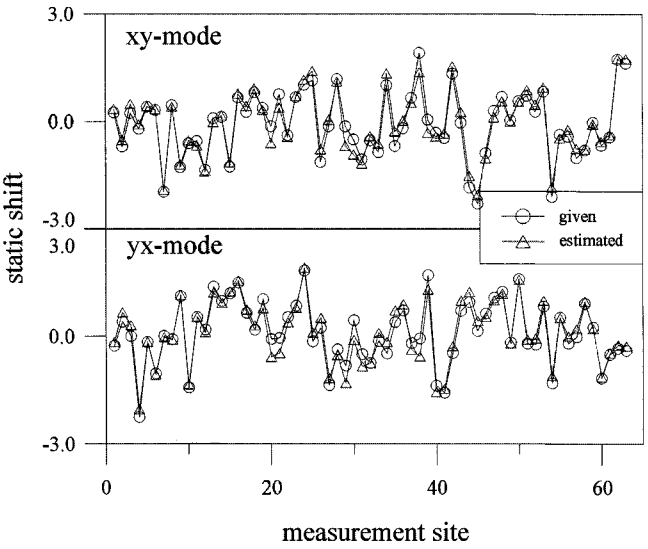

Fig. 9. Estimated static shift parameters for the dataset2, 9 % random Gaussian static shifts are added. Note that the estimated static shift closely approaches to the given values even in the case that the data are affected by strong static shifts.

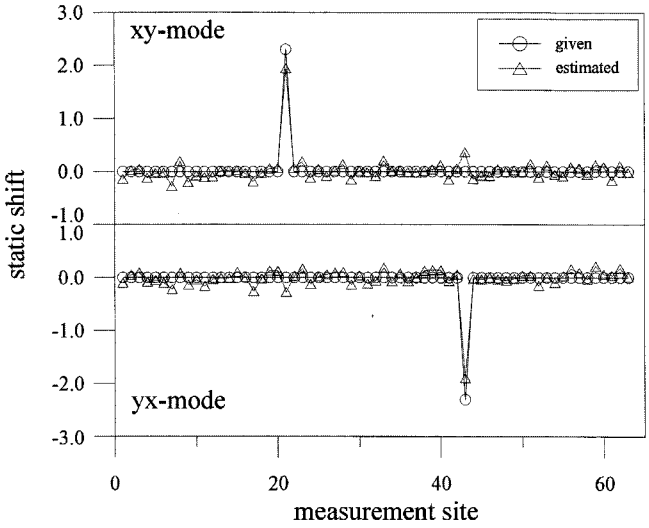

Fig. 10. Estimated static shift parameters for the dataset3. The static shifts are occurred only in yx-mode of Site 43 and the inversion successfully estimates the static shift with non-Gaussian distribution.

site number 43. The given static shift is -2.3, which corresponds to 0.1 times of its apparent resistivity. The estimated static shift is -1.9, which corresponds to 0.14 times at site 43 and all others approach nearly zero. Though it shows slightly bigger estimation of static shift in xy-mode of site 43, overall estimation is quite well matched with given ones.

Concluding remarks

Galvanic distortion by small-scale shallow feature will

lead severe distortion in inverted resistivity structures. Removing static shift is a critical problem and will vastly improve interpretation of MT data. In conventional MT survey we usually do not have any additional information about static shift. Simultaneous inversion of block resistivity and static shift parameters is an alternative to deal with the problem. In such case the determination of appropriate weighting for static shift parameter and the smoothness constraint is important.

In this study, characteristics of static shift in 3-D MT inversion are discussed using a model test with different static shift contents. Simultaneous searching for appropriate weighting for both static shift parameters and the model smoothness based on the rms misfits at each iteration, showed quite reasonable estimate of the amount of the static shift components contained in the data. The 3-D inversion with static shift parameterization efficiently separates the Gaussian static shifts in the data, and even when the static shift does not obey the Gaussian distribution. Allowing the degree of freedom by the static shift parameters, the inversion could get more accurate block resistivities as well as given static shifts.

When the inversion does not consider the static shift as inversion parameters, the block resistivities on the surface are modified considerably to match possible static shift. By those mechanisms, the conventional 3-D MT inversion can reconstruct the resistivity structures in deeper parts, when the static shift is not so strong (Dataset1). As frequency increased, however, the galvanic distortion is not frequency independent any more, and thus the conventional inversion failed to fit the apparent resistivity and phase, especially when strong static shift is added. Even in such case, however, reasonable estimation of block resistivity as well as static shift parameters were obtained by 3-D MT inversion with static shift parameterization.

Acknowledgments

The authors are grateful to Dr. Yasuo Ogawa for his helpful suggestion during the work and to JISTEC for financial support. TJL was partly supported by KORP (Korea Research Council of Public Science & Technology) funding to KIGAM (Korea Institute of Geoscience and Mineral Resources). TJL and TU used a computer system at the Tsukuba Advanced Computer Center, AIST.

References

Bostick, F. X., 1986, Electromagnetic Array Profiling (EMAP): 56th Ann. Mtg., Soc. Expl. Geophys., *Expanded Abstracts*, 60-61.

deGroot-Hedlin, C., 1991, Removal of static shift in two dimensions by regularization inversion: *Geophysics*, **56**, 2102-2106.

Groom, R. W. and Bailey, R. C., 1989, Decomposition of magnetotelluric impedance tensors in the presence of local three-dimensional galvanic distortion: *J. of Geophys. Res.*, **94**, 1913-1925.

Jones, A. G., 1988, Static shift of magnetotelluric data and its removal in a sedimentary basin environment: *Geophysics*, **53**, 967-978.

Kurtz, R. D., Craben, J. A., Niblett, E. R., and Stevens, R. A., 1993, The conductivity of the crust and mantle beneath the Kapuskasing Uplift - electrical anisotropy in the upper mantle: *Geophys. J. Int.*, **113**, 483-498.

Le Mouel, J. L., and Menvielle, M., 1982, Geomagnetic variation anomalies and deflection of telluric currents: *Geophys. J. R. Astr. Soc.*, **68**, 575-587.

Ogawa, Y. and Uchida, T., 1996, A two-dimensional magnetotelluric inversion assuming Gaussian static shift: *Geophys. J. Int.*, **126**, 69-76.

Romo, J. M., Flores, C., Vega, R., Vazaquez, R., Perez-Flores M. A., Gomez-Trevino, E., Espaarza, F. J., Quijano, J. E., and Garcia, V. H., 1997, A closely-spaced magnetotelluric study of the Ahuachapan-Chipilapa geothermal field, El Salvador: *Geothermics*, **26**, 627-656.

Sasaki, Y., 1999, Three-dimensional frequency-domain electromagnetic modeling using the finite-difference method: *Butsuri-Tansa*, **52**, 421-431.

Sasaki, Y., 2001, Three-dimensional inversion of static-shifted magnetotelluric data: *Proc. 5th SEGJ International Symposium*, 185-190.

Sternberg, B. K., Washburne, J. C., and Pellerin, L., 1988, Correction for the static shift in magnetotellurics using transient electromagnetic soundings: *Geophysics*, **53**, 1459-1468.

Torres-Verdin, C., 1991, Continuous profiling of Magnetotelluric Fields: Ph. D thesis, Univ. of California Berkeley.

Uchida, T., Ogawa, Y., Takakura, S., and Mitsuhata, Y., 2000, Geoelectric investigation the Kakkonda geothermal field, northern Japan, *Proceedings World Geothermal Congress 2000*, 1893-1898.

Uchida, T., Lee, T. J., Honda, M., Ashari, and Andan, A., 2001, 2-D and 3-D interpretation of magnetotelluric data in the Bajawa geothermal field, central Flores, Indonesia: Research report, Geological Survey of Japan.

Wannamaker, P. E., Hohmann, G. W., and Ward, S. H., 1984, Magnetotelluric responses of three-dimensional bodies in layered earths: *Geophysics*, **49**, 1517-1533.